



Low-temperature in-situ growth of SnO₂ nanosheets and its high triethylamine sensing response by constructing Au-loaded ZnO/SnO₂ heterostructure

Ting Zhai, Hongyan Xu*, Wenru Li, Huanqin Yu, Zhengrun Chen, Jieqiang Wang,
Bingqiang Cao*

School of Materials Science and Engineering, University of Jinan, Jinan 250022, Shandong, China



ARTICLE INFO

Article history:

Received 22 October 2017

Received in revised form

30 November 2017

Accepted 3 December 2017

Available online 5 December 2017

Keywords:

Au@ZnO/SnO₂ nanosheet

Directly grown

Schottky contact

Heterojunction

TEA gas sensing

ABSTRACT

In this report, uniform SnO₂ nanosheets (NSs) have been in-situ grew on the surface of Al₂O₃ tubes via a cost-efficient hydrothermal synthesis at low temperature. The nanostructures of ZnO/SnO₂ were prepared by employing pulsed laser deposition (PLD) method. Furthermore, Au surface modification with DC-sputtering process is used to improve the sensitivity of ZnO/SnO₂ NSs sensor to TEA gas. The Au@ZnO/SnO₂ NSs exhibited high response ($S = 115$) to 100 ppm trimethylamine (TEA) gas at 300 °C, which was about 20 times higher than that of the pristine SnO₂ NSs. The enhanced sensing properties of Au@ZnO/SnO₂ NSs sensor are discussed from the points of Au@ZnO Schottky contact and ZnO/SnO₂ n-n heterojunction on the basic of depletion layer model.

© 2017 Elsevier B.V. All rights reserved.

1. Introduction

Triethylamine (TEA), as a volatile organic compound, is widely used as organic solvents, catalyst, preservatives, and synthetic dyes [1]. However, TEA is also toxic, volatile, inflammable, and explosive, which easily generates risks to environment. Moreover, it is also a gaseous organic amine given off during the decay of fishes and seashells after death, and the concentration of TEA increases with the decreasing freshness of fishes [2,3]. According to National Institute for Occupational Safety and Healthy (NIOSH) recommended, the permissible exposure limited concentration of TEA is 10 ppm in the workplace [4]. Therefore, there is an urgent need to develop new TEA sensors with high response and good selectivity for the biomedical, chemical, food industries, and also our daily life [5].

It is well known that the both high sensitivity and selective detection are the most important parameters in gas sensors performance [6–10]. Meanwhile, metal oxide semiconductors (MOSS)

are a promising functional material for gas sensors with several advantages which include cost-efficient, simple fabrication, and good stability [11]. MOSSs such as ZnO [12], SnO₂ [13,14], Fe₂O₃ [15,36], and MoO₃ [16] have been extensively investigated for gas sensor applications. As one important kind of sensing material, SnO₂ has been extensively studied due to its high electron mobility, superior chemical properties, and good response toward various gases [17,18]. However, pure SnO₂ (with a direct band gap of 3.6 eV) sensors have its drawbacks, including low response, pure selectivity, and high working temperature. Work in more complicated systems and under more harsh conditions, there is insufficient application to meet demand [19,20]. Up to now, composites consisting of two or more metal/metal oxides heterojunction structures have gained extensive attention to indeed improve the sensing properties [21–25]. For example, Xu et al. [26] prepared TiO₂/SnO₂ n-n heterojunction nanosheets, and the response of its sensor was higher than that of pure SnO₂ sensor. Moreover, decorated with Au nanoparticles could also enhance the sensing performances of MOSs based sensors [27]. Li et al. [28] synthesized Au@SnO₂ yolk-shell nanospheres, and their response to 100 ppm of acetone was about 2–3 times higher than that of SnO₂ nanospheres.

Inspired by the above works, we designed and fabricated ternary Au@ZnO/SnO₂ NSs sensors. The pure SnO₂ NSs directly

* Corresponding author. School of Materials Science and Engineering, University of Jinan, Jinan 250022, PR China.

** Corresponding author.

E-mail addresses: mse_xuhy@ujn.edu.cn (H. Xu), [\(B. Cao\).](mailto:mse_caobq@ujn.edu.cn)

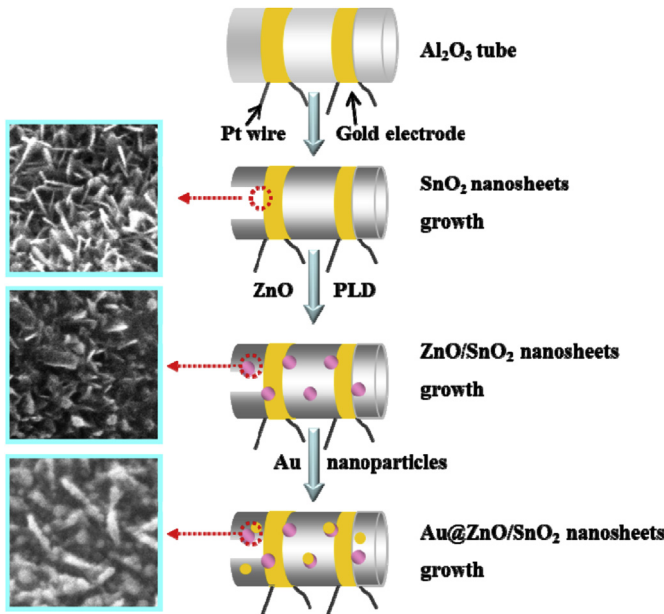


Fig. 1. Schematic of the grow process of Au@ZnO/SnO₂ NSs.

grown on Al₂O₃ tubes by a simple hydrothermal synthesis method, which overcome the shortcomings from the traditional slurry coating process in term of time-consuming and destroyed the intrinsic physical nanostructure [15,16,29]. Then, the ternary Au@ZnO/SnO₂ NSs sensors are obtained through ZnO and Au surface depositing. Moreover, the gas sensing performances of the sensors toward TEA were comprehensively studied. Compared with other two sensors, the test results show that the Au@ZnO/SnO₂ NSs sensor exhibits greatly high gas response ($S = 115$) for 100 ppm TEA gas at 300 °C. In the final section the mechanism of the enhanced sensing properties of Au@ZnO/SnO₂ NSs was discussed in detail.

2. Experimental sections

All chemicals were purchased from Sinopharm Chemical Reagent (Shanghai, China) and used without further purification. The schematic diagram of the Al₂O₃ tube is shown in Fig. 1, which has three basic components including Pt wires, gold electrodes, and ceramic tube. Moreover, Fig. 1 schematically illustrates the fabrication process of the Au@ZnO/SnO₂ NSs sensor, which has been

described in detail on section 2.1 and 2.2 of experimental sections.

2.1. Direct growth of SnO₂ NSs on Al₂O₃ tubes

The SnO₂ NSs were synthesized by low-temperature hydrothermal way. In a typical preparation of SnO₂ NSs structures, 0.1 M SnCl₂·2H₂O solution were add into 0.1 M CO(NH₂) solution under vigorous stirring for about 20 min. In brief, a cleaned Al₂O₃ tube was placed in a Teflon-lined stainless steel autoclave, then the final mixture was also transferred into Teflon-lined, maintained at 95 °C for 24 h. And these were allowed to cool to ambient temperature in the air, what obtained in this moment is SnO. The samples were dried at 70 °C in an oven then annealed at 500 °C for 30 min in a furnace to form SnO₂ NSs on Al₂O₃ tube directly.

2.2. Growth of ZnO/SnO₂ NSs and loading of Au nanoparticles

ZnO nanoparticles were deposited onto the surface of SnO₂ NSs by pulsed laser deposition (PLD) method in a vacuum at room temperature. Using ZnO target deposition, a binary structure of ZnO/SnO₂ was formed on Al₂O₃ tube. Where after, Au nanoparticles were sputter on the surface of ZnO/SnO₂ NSs by DC sputtering, which was obtained Au@ZnO/SnO₂ NSs.

2.3. Material characterizations and sensor properties testing

The morphology of the samples was investigated by a field emission scanning electron microscope (FESEM, FEI QUANTA FEG250) and a transmission electron microscope (TEM, JEM-2100F, JEOL). Elemental analysis was performed by energy dispersive spectroscopy (EDS, INCA MAX-50) integrated into the FESEM system. The phase and surface elemental composition of sensing materials, was checked with X-ray diffraction (XRD, D8-Advance, Bruker) and X-ray photo-electron spectroscope (XPS, Thermo ESCALAB 250XI), respectively. The gas sensing properties of the sensor were tested with the gas-sensing test system (WS-30A, Weisheng Electronics, China). The devices were put into an airproof test box. Target gases such as TEA with calculated concentration were injected into the testing chamber by a microsyringe. Here, the gas sensing response is defined as the ratio of the resistance in air (R_a) to that of the resistance in target gas (R_g) [3,30]. The response and recovery time was defined as needed time spans to reach a 90% variation in resistance of the difference from the maximum after injecting and removing the detected gas [31].

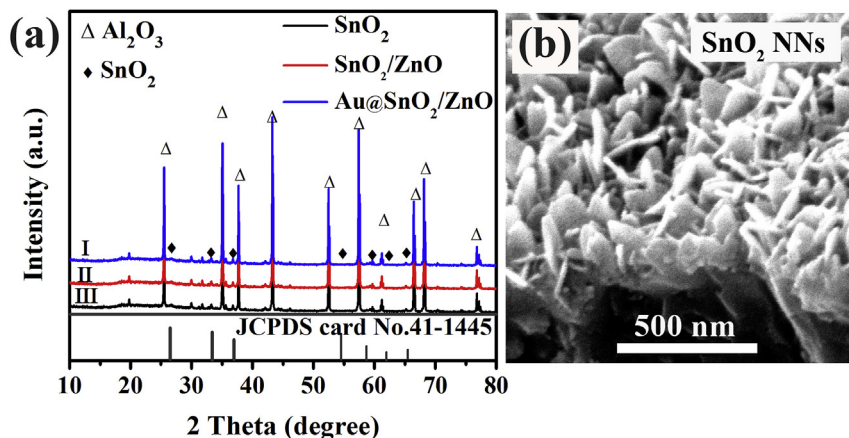


Fig. 2. (a) The XRD patterns of SnO₂, ZnO/SnO₂, and Au@ZnO/SnO₂ NSs. (b) SEM image of SnO₂ nanosheet in cross-sectional view.

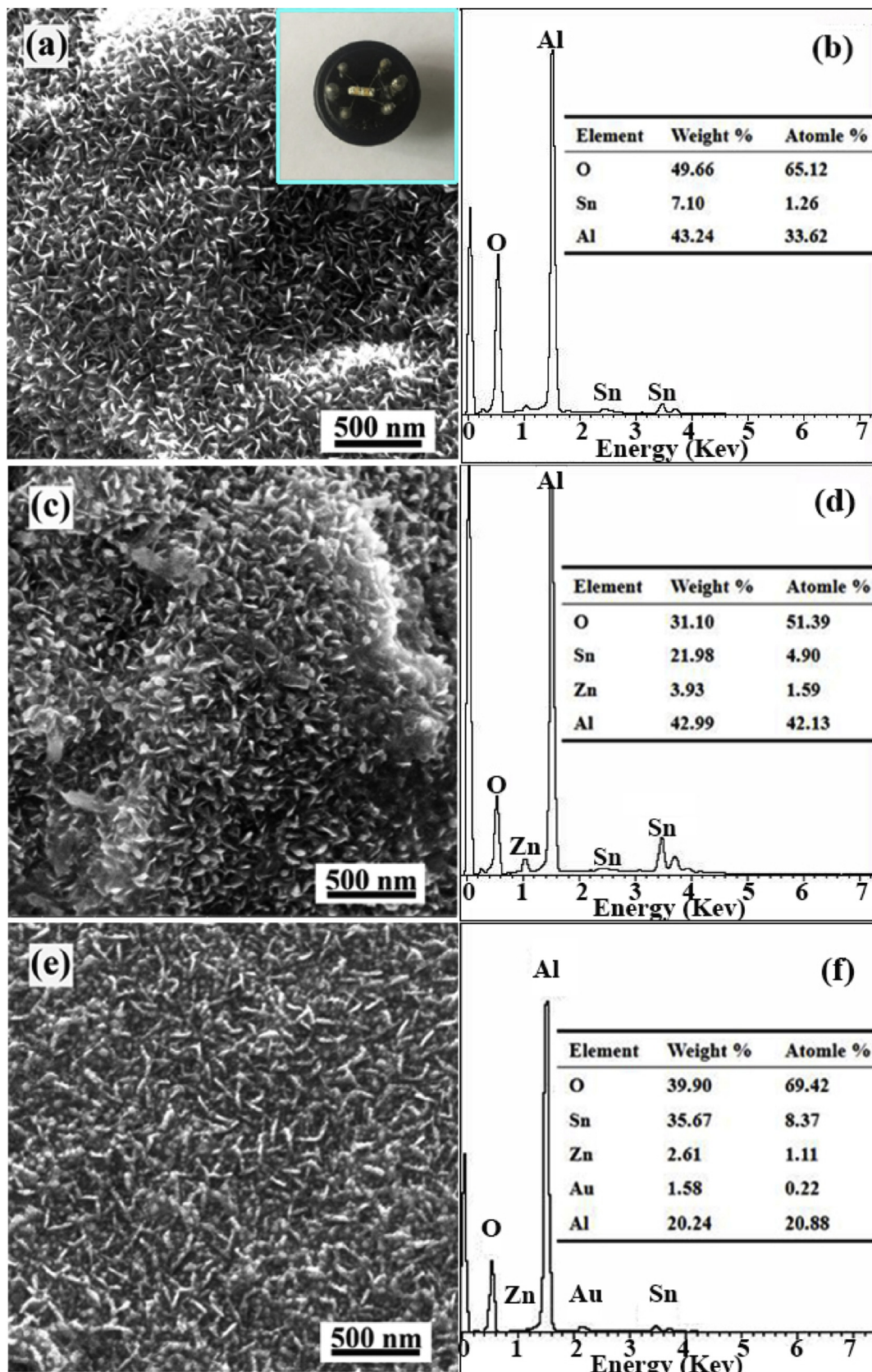


Fig. 3. (a) SEM morphologies of SnO_2 (inset pattern) gas sensor fixed on an electronic bracket, (b) EDS spectrums of SnO_2 . The SEM morphologies and EDS spectrums of (c,d) ZnO/SnO_2 , (e,f) $\text{Au}@\text{ZnO}/\text{SnO}_2$ NSSs.

3. Results and discussion

3.1. Characterizations of SnO_2 -based NSs

The crystal of SnO_2 -Based NSs was characterized by XRD. Fig. 2a shows the XRD pattern of obtained SnO_2 , ZnO/SnO_2 , and $\text{Au}/\text{ZnO}/\text{SnO}_2$ samples. The XRD pattern of the SnO_2 NSs can be indexed to a SnO_2 phase (JCPDS Card No. 41-1445). Compared with the strong peaks of Al_2O_3 substrate, those of SnO_2 phase are relatively weaker. When Au and ZnO were deposited onto SnO_2 NSs, the XRD peaks of Au and ZnO could not be observed due to the low contents of Au and ZnO. Fig. 2b reveals that sheet-like SnO_2 in-situ grow on the substrate, evidenced by cross-sectional image.

Seeing from Fig. 3a, one can find that the diameter of the SnO_2 NSs is about 200–500 nm, and the distribution of in-situ SnO_2 NSs

are relatively uniform and the insert shows the optical photograph of $\text{Au}/\text{ZnO}/\text{SnO}_2$ gas sensor. The peak of O and Sn can be clearly observe in this spectrum as shown in Fig. 3b and no peaks are observed for other impurities, confirming the growth of pure SnO_2 . As can be seen from Fig. 3c, SEM morphology of ZnO/SnO_2 NSs sample shows that the nanosheets of the ZnO/SnO_2 samples are thicker than that of pure SnO_2 samples. The reason is that the ZnO/SnO_2 NSs sample is prepared by depositing with ZnO on pure SnO_2 NSs. According to the SEM morphologies shown Fig. 3e, it can be seen that gold particles attach themselves to the surface of ZnO/SnO_2 NSs samples. As can be analyzed in Fig. 3 (d,f), peaks of Al observed in the spectrum are attributed to the Al_2O_3 tubes. Although the contents of Au and Zn are relatively small, the peaks of Au and Zn were also observed. Ultimately, it can be concluded that the surface of pure SnO_2 sample is covered with ZnO and Au

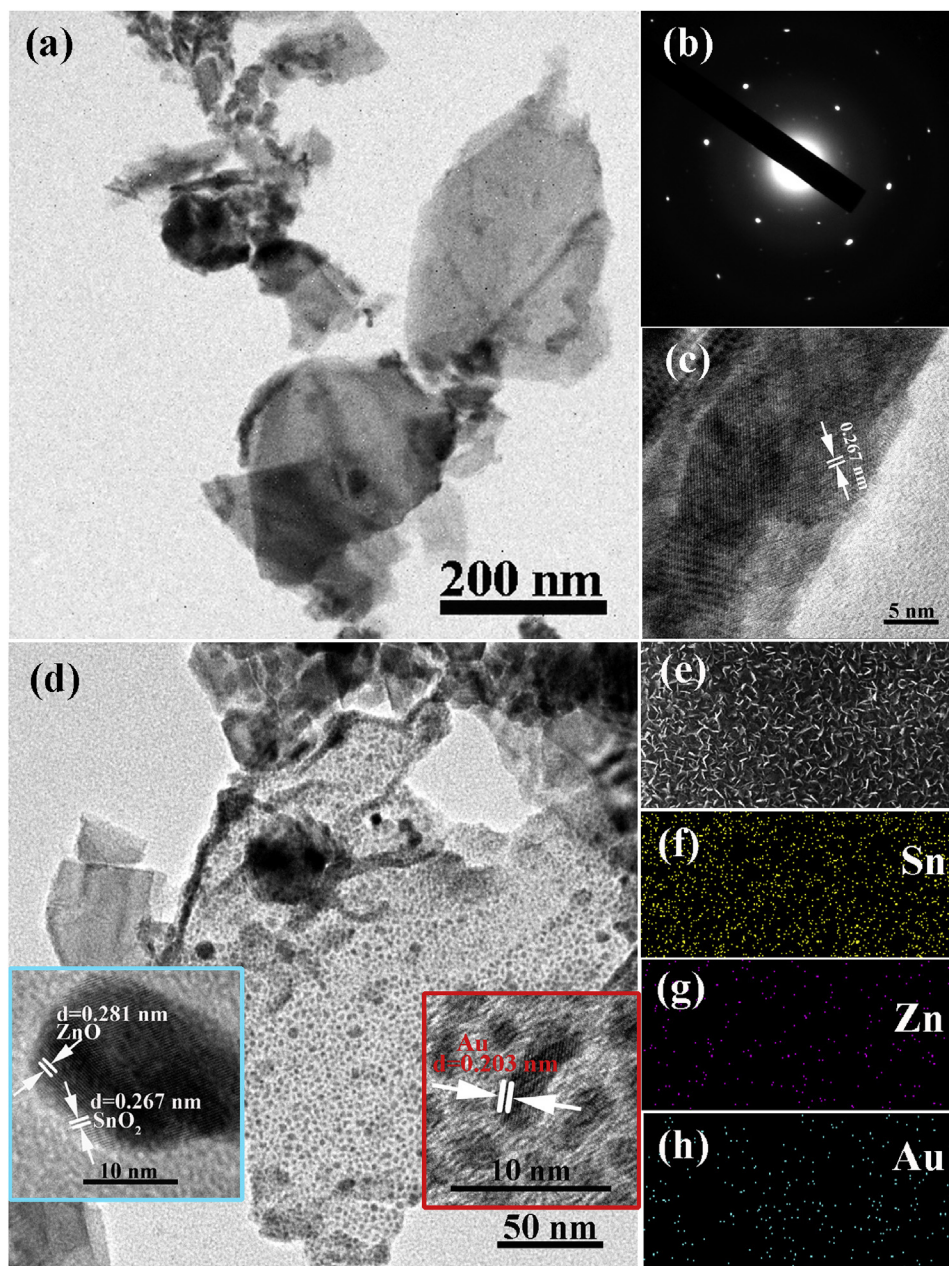


Fig. 4. (a) TEM image, (b) corresponding SAED pattern and (c)HRTEM image of SnO_2 NSs. (d) TEM image of $\text{Au}/\text{ZnO}/\text{SnO}_2$ NSs, the insert are HRTEM images for the corresponding region. (e)The SEM image and (f–h) EDS patterns of $\text{Au}/\text{ZnO}/\text{SnO}_2$ NSs.

materials.

The SnO₂ lattice fringes seen in HRTEM image shown in Fig. 4c and single crystalline structure of the SnO₂ NNs illustrated in the SAED pattern of Fig. 4b. TEM image shows the SnO₂ and ternary NSs, which are made up of monodispersed sheet-like nanocomposite (Fig. 4 a,d). These indicate that the following experiment, after ZnO and Au deposition, has no effect on morphology of sheet SnO₂. The interconnected nanocrystals obtained at even higher magnifications show lattice fringes that can be identified with crystallographic planes of the SnO₂, ZnO and Au phases, respectively. In Fig. 4d, the blue-colored frame insert, represents inter planar distances of 0.267 and 0.281 nm, representing the SnO₂ and ZnO. The red insert, displaying lattice fringes of 0.203 nm, assigned to (200) plane of Au. As we can see in Fig. 4(f–h), there are three elements: Sn, Zn and Au in Au@ZnO/SnO₂ NSs. We can also find that the ZnO and Au nanoparticles are evenly loaded on the surface of SnO₂. These dates are in good agreement with that ZnO and Au are

exactly combined to SnO₂ NSs.

In order to obtain more detailed surface chemical compositions and their electronic states of the elements, the as-synthesized Au@ZnO/SnO₂ microstructure was further characterized by XPS. Fig. 5a shows the XPS full survey spectrum of the sample, in this picture, the peaks of Zn, Sn, Au, O, and C elements can be observed clearly. The plans b, c, and d of Fig. 5 display the high-resolution spectra for Sn, Zn, and Au species, respectively. Fig. 5b reveals three peaks at 495.01, 486.43, and 498.2 eV, corresponding to Sn (loss), Sn 3d_{3/2}, and Sn 3d_{5/2}. Binding energy of Sn 3d_{5/2} was similar to that of Sn⁴⁺ in SnO₂, and higher than Sn²⁺ in SnO or Sn [32,33]. The results exhibit that Sn⁴⁺ are stable. The peaks of Fig. 5c are centered at 1021.6 and 1044.7 eV, which are attributed to the Zn 2p_{3/2} and Zn 2p_{1/2} of Zn element. In Fig. 5d, there are two peaks in the Au 4f region. The peak located at 87.8 eV corresponds to the Au 4f_{5/2} and another one located at 84.1 eV is assigned to Au 4f_{7/2}. While the high-resolution XPS O1s peak was fitted using three

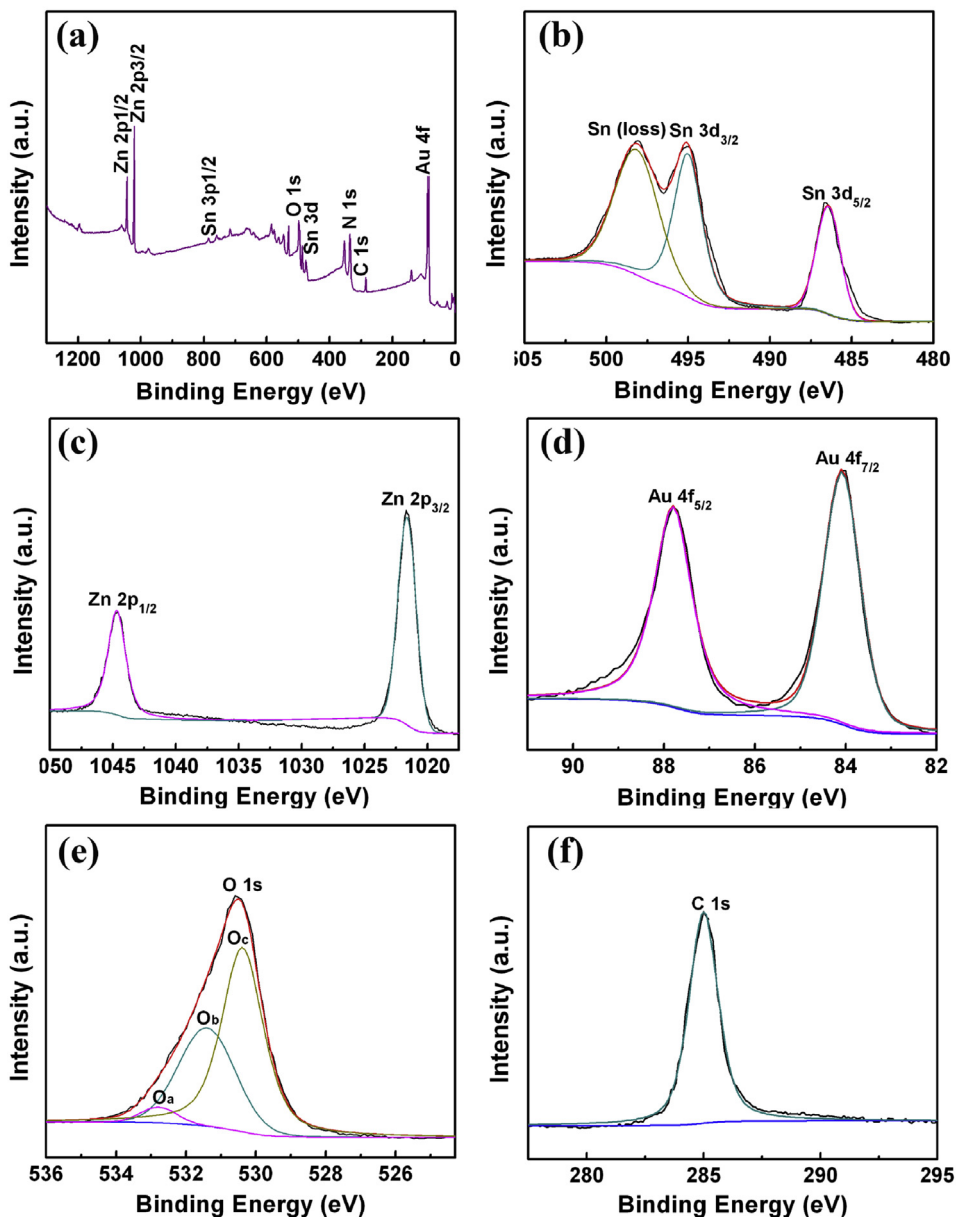


Fig. 5. XPS survey spectra and fitted data of the as obtained Au@ZnO/SnO₂ NSs: (a) full survey spectrum, (b) Sn 3d spectrum, (c) Zn 2p spectrum, (d) O 1s spectrum, (e) Au 4f spectrum and (f) C 1s spectrum.

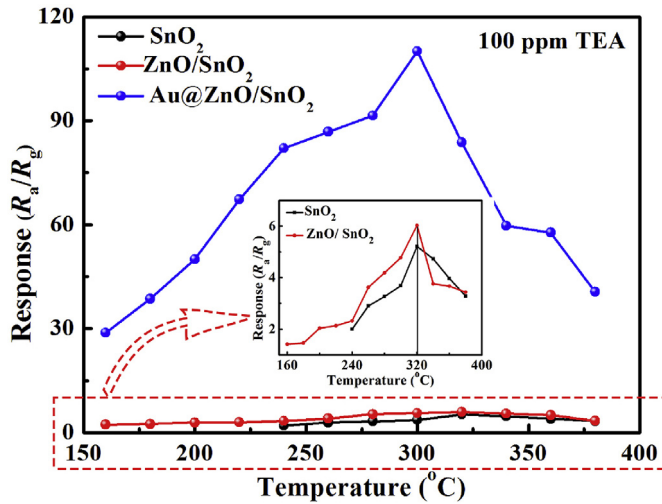


Fig. 6. Gas responses of SnO_2 , ZnO/SnO_2 , and $\text{Au}@\text{ZnO}/\text{SnO}_2$ sensor to 100 ppm of TEA at different operating temperature (160–400 °C). The inset is the larger image of the red frame. (For interpretation of the references to color in this figure legend, the reader is referred to the Web version of this article.)

simulated Gaussian peaks are shown in Fig. 5e. Thus, in order to make the situation about structural properties more clear, the O1s peak was fitting into three peaks at 532.8 (labeled at O_a), 531.4 (marked as O_b), and 530.4 (labeled at O_c) eV, respectively. Based on previous reports, O_a can be corresponded to surface oxygen, identified as chemisorbed oxygen species. O_b represented the surface active oxygens that reflect on generated oxygen vacancies [34]. O_c was attributable to O^{2-} in the SnO_2 which form the $O-\text{Sn}^{4+}$ bonding [35]. The high-resolution XPS spectrums of and C 1s (Fig. 5f) show peaks at 284.7 eV, the existed of carbon is due to surface carbon contamination of the sample in open air.

3.2. Gas sensing properties

The response of SnO_2 -based NSs sensors to 100 ppm TEA measured at different working temperatures are shown in Fig. 6. With increasing operating temperature, the sensitive of all sensors increases first and then decreases, hence the maximum response of $\text{Au}@\text{ZnO}/\text{SnO}_2$ NSs sensor to 100 ppm of TEA is about 115 at a higher temperature of 300 °C. It is worth noting that the $\text{Au}@\text{ZnO}/\text{SnO}_2$ sensor exhibits greater response than the above other sensors (pure SnO_2 and ZnO/SnO_2 sensor). Meanwhile, the response of binary combination sensors (ZnO/SnO_2 sensor) is slightly higher than pure SnO_2 sensor, which also can be observed clearly in the inset of Fig. 6. Compared to SnO_2 and ZnO/SnO_2 sensor, $\text{Au}@\text{ZnO}/\text{SnO}_2$ NSs sensor exhibits not only lower optimal operating temperature but also greatly higher sensitivity.

At fixed sensor temperatures, the gas concentration may also influence the sensing response [36]. We measured the TEA sensing response in the range of 2–1000 ppm at 300 °C. The trend is that the response of each sensor increases with increasing TEA concentration, as shown in Fig. 7 (a,b). Besides, this figure shows that the response value of ZnO/SnO_2 NSs sensors is higher than that of SnO_2 NSs sensors. As the same time, the $\text{Au}@\text{ZnO}/\text{SnO}_2$ NSs sensors response can reach to 115, which is far stronger than that of pristine SnO_2 sensors with gas concentration of 100 ppm. The response of $\text{Au}@\text{ZnO}/\text{SnO}_2$ NSs sensor is about 37 times larger than pure SnO_2 sensor which can also be observed more clearly from Fig. 7b. It illustrates that the response of all sensor rises faster with the increase of TEA concentration. However, gas concentration from 500 to 1000, the sensitivity of all the devices changed a little, the cause

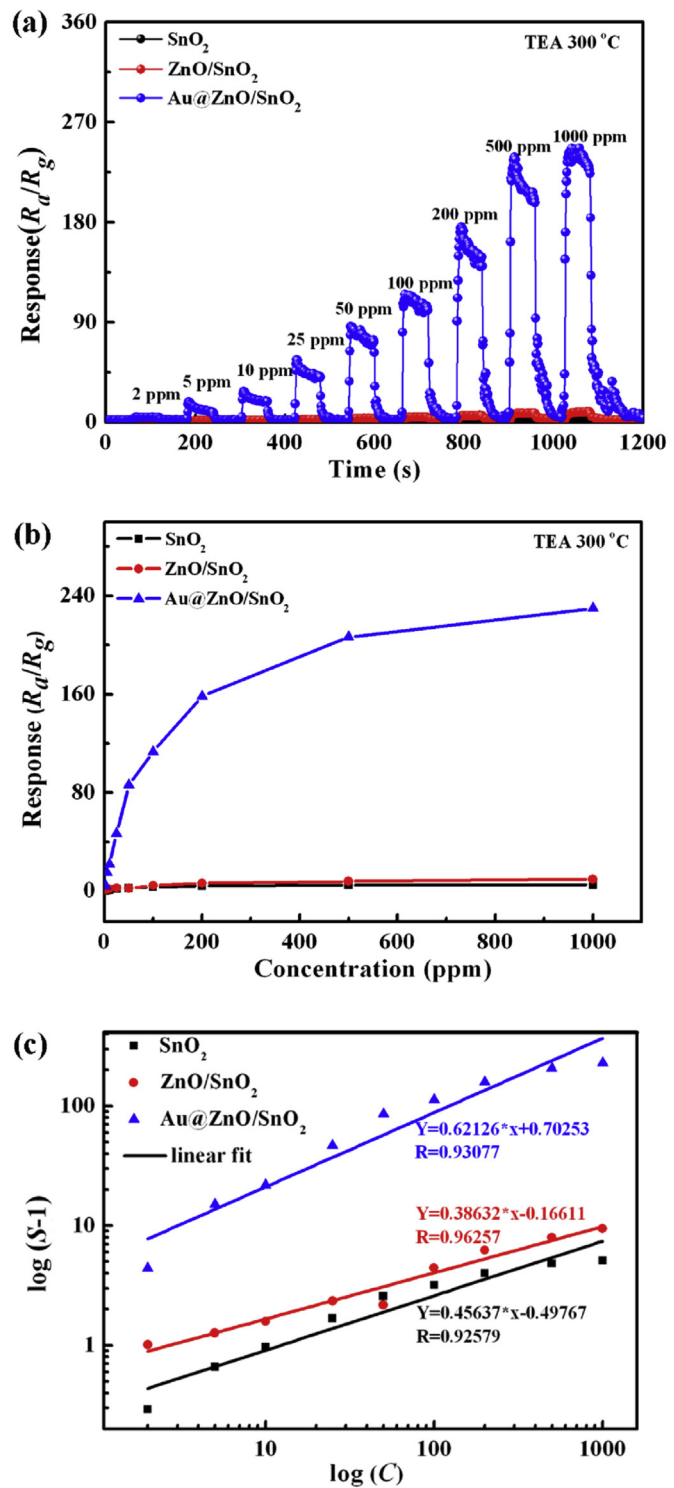


Fig. 7. (a) Response and recovery curves of three kinds of sensors to TEA gas of different concentration at 300 °C. (b) corresponding relationship between sensor response and TEA concentration. (c) the $\log (S-1)$ versus $\log (C)$ plot of three sensors for TEA gas and the corresponding linearly fitted results.

may be the gas molecules involved in the reaction to the saturation on the sensor surface. Fig. 7c manifests the linear relationship of $\log (S-1)-\log (C)$ plot to TEA. This equation, $S = a[C]^b + 1$, represents the relationship between response of gas sensor and concentration. In this formula, a and b are the constants, S is the gas response, and C is the concentration of TEA. The slopes of pure SnO_2 NSs and ZnO/SnO_2 NSs sensors are similar, while the slope of $\text{Au}@\text{ZnO}/\text{SnO}_2$ NSs sensor is much steeper, indicating a higher sensitivity to TEA.

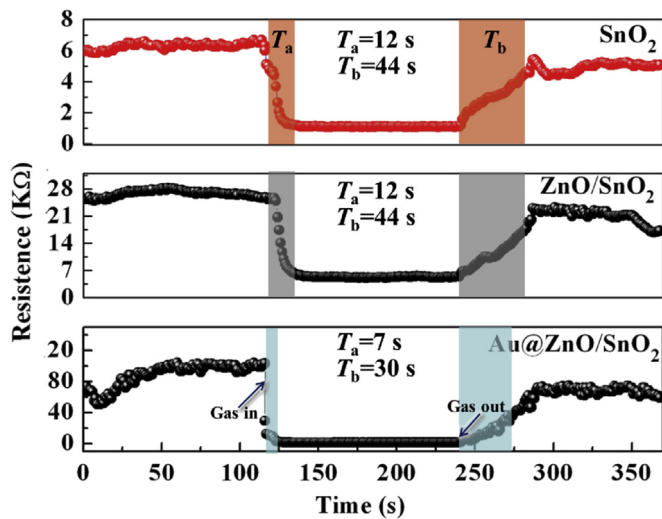


Fig. 8. The response-recovery of (a) SnO_2 NSs, (b) ZnO/SnO_2 NSs, and (c) $\text{Au}@\text{ZnO}/\text{SnO}_2$ NSs sensor to 100 ppm TEA at 300 °C.

SnO_2 NSs and $\text{Au}@\text{ZnO}/\text{SnO}_2$ NSs based sensors are 0.92579, 0.96257, and 0.93077, respectively. These results indicate that the gas response of all sensor exhibits well linear characteristic with increasing gas concentration.

A fast response-recovery is important for the gas sensors in target gas analysis [30]. Fig. 8 shows response-recovery characteristics of three kinds of sensors operating at 300 °C to 100 ppm TEA. According to the above definition of response and recovery time, it can be clearly observed from Fig. 8. The response time (T_a) of SnO_2 , SnO_2/ZnO , and $\text{Au}@\text{ZnO}/\text{SnO}_2$ sensor are 12, 12, and 7 s respectively. Moreover, the recovery time (T_b) of SnO_2 , ZnO/SnO_2 , and $\text{Au}@\text{ZnO}/\text{SnO}_2$ sensor are 44, 44, and 30 s, respectively.

A typical response profiles to investigate repeatability of the gas

sensors after aged for 36 h in Fig. 9a. It is noted that every sensor is in good reproducible run after five cycles, indicating a very good repeatability of the sensors. Meanwhile, seeing from Fig. 9b, the selective capacities of the SnO_2 , ZnO/SnO_2 , and $\text{Au}@\text{ZnO}/\text{SnO}_2$ sensors were tested to 100 ppm various gases (benzene, p-xylene, acetone, ethanol, isopropanol, triethylamine) identified by TEA detection. Testing results indicate that the $\text{Au}@\text{ZnO}/\text{SnO}_2$ sensors have excellent selectivity and high sensitivity towards TEA. One possible reason may be that the low bond energy of C=N for TEA molecules has high reaction activity. C=N bonds is easier to broken which is probably contributed to the high response of $\text{Au}@\text{ZnO}/\text{SnO}_2$ sensors. A comparison between the sensing performances of $\text{Au}@\text{ZnO}/\text{SnO}_2$ nanosheet sensors and the TEA gas sensors of literature reported is summarized in Table 1 [3,25,37,40,42]. It is noteworthy that our sensors exhibit higher response than other nanostructured SnO_2 sensors.

3.3. The mechanism of the enhanced sensing properties

The experiments show that gas sensors made of SnO_2 NSs, ZnO/SnO_2 hetero-nanosheets and $\text{Au}@\text{ZnO}/\text{SnO}_2$ NSs are all sensitive to TEA. And the response value of $\text{Au}@\text{ZnO}/\text{SnO}_2$ sensor is far larger than both ZnO/SnO_2 and SnO_2 NSs sensor. When the semiconductor heterojunctions such as n-n, n-n, or metal/semiconductor contact are formed on the surface of the sensing material, the results of enhanced sensor properties are already reported [37–39]. However, the mechanism of gas sensing properties becomes rather complex and remains unclear, especially the mechanism of the enhanced sensing properties.

Fig. 10a shows the energy band diagrams of ZnO , SnO_2 and Au . The work function of SnO_2 (W_s), ZnO (W_z) and Au (W_m) are 4.9, 5.2, 5.4 eV, respectively [40–43]. As we all known, the working mechanism of the gas sensor relies on transport of electrons due to surface reactions namely oxidation or reduction reactions with different gas exposures [44]. As illustration in Fig. 10c, when the

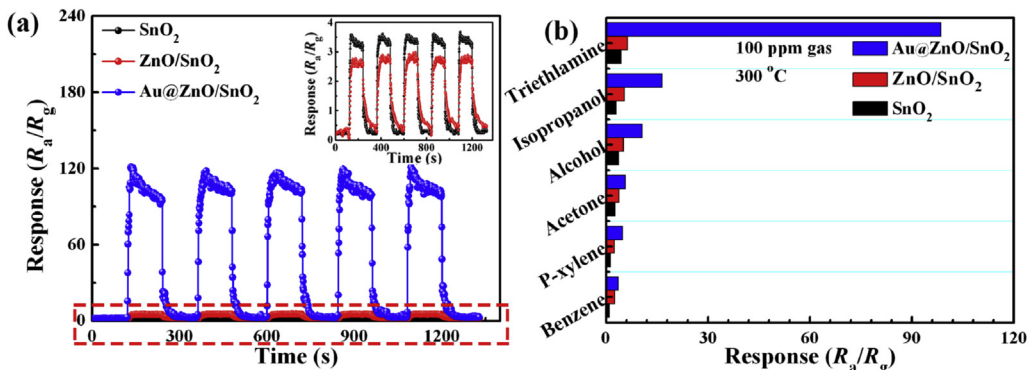


Fig. 9. (a) Selectivity of three sensors for different target gases: benzene, p-xylene, acetone, ethanol, isopropanol, triethylamine with same concentration at 300 °C. (b) Repeatability test of the sensors to 100 ppm of TEA at 300 °C. The illustration is the larger image of the red frame. (For interpretation of the references to color in this figure legend, the reader is referred to the Web version of this article.)

Table 1

TEA sensing properties of our work and other reported stannic oxide semiconductor gas sensors working under different operating temperatures.

Material	TEA (ppm)	Operating temperature (°C)	Response (R_a/R_g)	Response/Recovery times (s)	Ref.
$\text{Au}@\text{ZnO}/\text{SnO}_2$ NSs	100	300	115	7/30	our work
hexagonal brick-shaped SnO_2	100	160	70	3/9	[3]
Au-SnO_2 nanosheets	50	40	7.1	~1.2/-70	[36]
$\text{TiO}_2/\text{SnO}_2$ nanosheets	100	260	52.3	12/22	[24]
NiO/SnO_2 hollow sphere	10	220	48.6	6/25	[33]
SnO_2 nanorods	1000	350	200	10/10	[38]

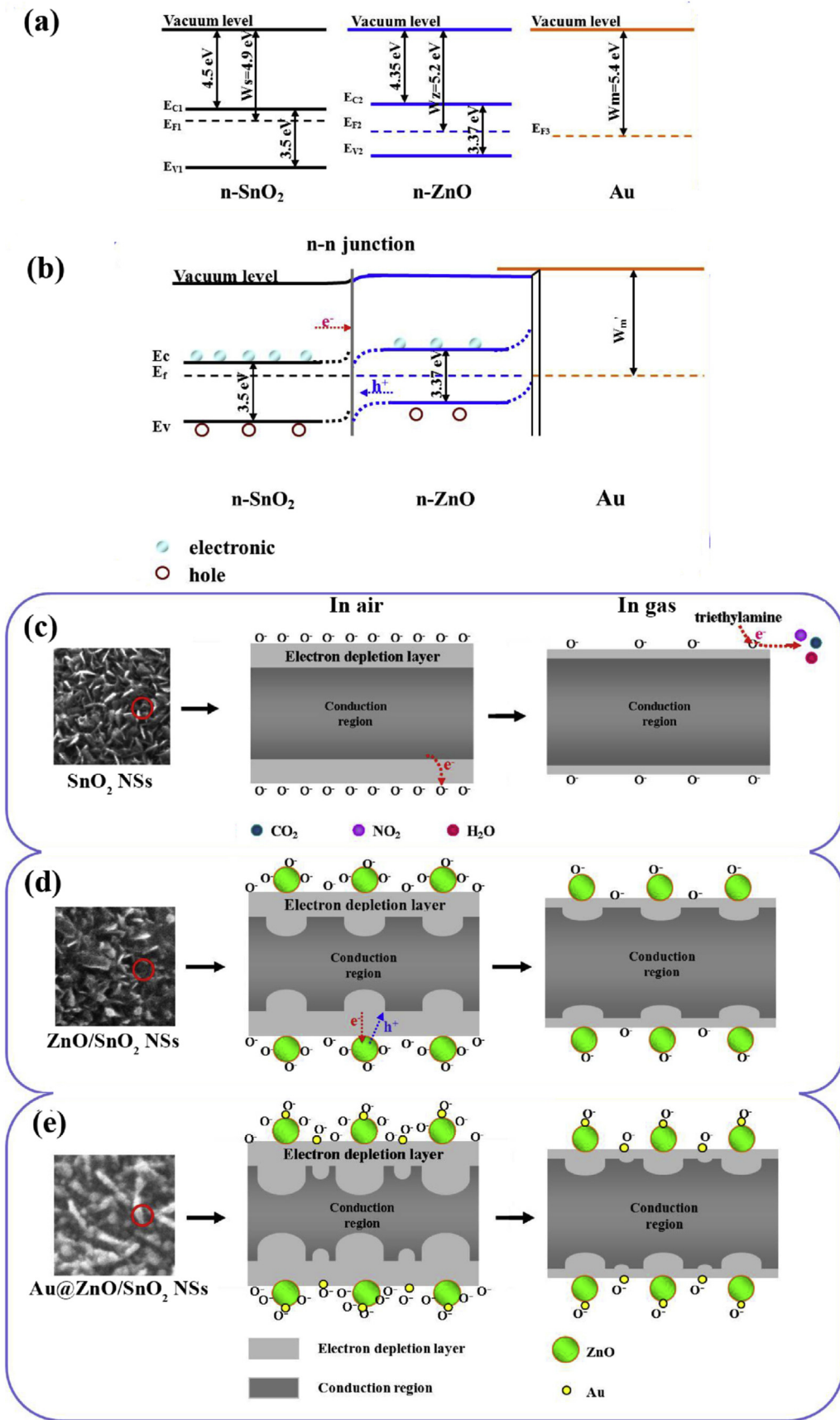
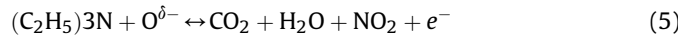


Fig. 10. Schematic diagrams of the TEA sensing mechanisms of (a) pure SnO₂, (b) binary ZnO/SnO₂, and (c) Au@ZnO/SnO₂ heterojunction NSs. (d) Schematic diagram of the energy band configurations for SnO₂, ZnO, and Au. (e) Energy band diagram of Au@ZnO/SnO₂ heterojunction.

SnO_2 sensors are exposed to air, oxygen molecules are adsorbed onto the surface of SnO_2 materials. The adsorbed oxygen molecules extract electrons from the conduction band, which creates an electron depletion layer at the surface of the SnO_2 nanosheets and can result in increasing of the SnO_2 NSs sensor's resistance [45]. That is to say, the value of SnO_2 sensor resistance increases in air (R_a). This progress can be described by following equations [46]:



When the SnO_2 based sensors were exposed to TEA gas, the reactions between the adsorbed oxygen and TEA on the surface of Au@ZnO/SnO_2 NSs sensors can be depicted as follows [20]:



The TEA molecules react with the oxygen ions, which results in electrons being released to the depletion layer and increasing the carrier concentration of SnO_2 . This decrease of resistance attributes to the fact that the reactions between surface adsorbed oxygen and target gases lead to decrease of depleted layer's thickness [47]. Similarly, ZnO/SnO_2 and Au@ZnO/SnO_2 sensor working principles in air and target gas are also schematically shown in Fig. 10.

Compared with pure SnO_2 NSs, the mechanism of the enhanced gas sensing of ZnO/SnO_2 NSs is as follows. Many studies have proven that semiconductor metal oxides with heterogeneous structure can significantly enhance gas sensing properties and are promising materials for gas sensor [48]. The improvement of the sensing properties of the ZnO/SnO_2 sensors to TEA gas may be attributed to formation of n-n heterojunctions between SnO_2 NSs and ZnO . It is well known that the work function of ZnO (5.2 eV) [40] is larger than SnO_2 (4.9 eV) [41,42]. Thus, in air, the electrons will flow from SnO_2 to ZnO until their Fermi levels equalize (schematically illustrated in Fig. 10b). Then, this creates an electron depletion layer on the surface of SnO_2 and further bends the energy band and leads to a slightly higher resistance state of sensing materials than that of the pure SnO_2 NSs sensor.

Furthermore, in comparison with ZnO/SnO_2 NSs, the mechanism of the enhanced gas sensing of Au@SnO_2 NSs is as follows. It has been reported that the work function of Au is 5.4 eV [43]. As shown in Fig. 10e, when Au nanoparticles are loaded on the surface of ZnO , electrons flow from ZnO to Au, which creates new depletion layer and further increases R_a . Similar to the interface of Au-ZnO , in the whole Au@ZnO/SnO_2 samples was deposited with Au, there also exists Schottky barrier between the interface of Au and SnO_2 NSs. Thus, there are further narrowed the conduction region in SnO_2 , leading to a high resistance of the Au@ZnO/SnO_2 sensor in air [49,50]. And based on the fundamental sensor response theory ($S=R_a/R_g$), the enhanced sensitivity (S) depends on the bigger resistance changes. Moreover, during the process of gas sensing, Au not only promotes electron transfer but also accelerates the kinetics of surface sensing reactions. That is to say, oxygen molecules can be more easily adsorbed on the surface of materials due to the sensitization effect of Au. The existence of ternary depletion layers in the NSs, which enhance a greater decrease in resistance upon exposure to TEA.

4. Conclusions

In summary, we demonstrate enhanced gas sensing property of ternary structure based on Au@ZnO/SnO_2 . The pure SnO_2 NSs were in-situ grown on the surface of Al_2O_3 tubes through hydrothermal synthesis technique. By employing PLD and sputtering method, the highly controllable and reproducible Au@ZnO/SnO_2 NSs heterojunction is successfully built. It is the unique combination of Au@ZnO/SnO_2 nanosheet with transport of charge carriers from metal oxide semiconductors to Au. In terms of sensing properties test, the response of as-prepared Au@ZnO/SnO_2 sensor could reach up to 115 when exposed to 100 ppm TEA at 300 °C. Moreover, the enhanced sensing properties could be interpreted from the angle of building of n-n heterojunctions and Schottky contact. The depletion layer is formed due to the presence of Au-ZnO Schottky, Au-SnO₂ Schottky, and SnO₂/ZnO n-n heterojunction contact in Au@ZnO/SnO_2 NSs, which greatly increases the sensor resistance in comparison with a pristine SnO_2 NSs sensor. This is the main reason for the enhanced response to TEA gas. This study would be useful for the enhancement of gas sensing properties of metal oxide semiconductor materials.

Acknowledgements

This work is supported by Shandong Provincial Key Research and Development Program (No. 2017GGX10135), Shandong Provincial Science Foundation (No. ZR2014JL045), and Science Foundation of University of Jinan (No. XKY1504).

References

- [1] L. Xu, H.J. Song, J. Hu, Y. Lv, K.L. Xu, A cataluminescence gas sensor for triethylamine based on nanosized $\text{LaF}_3\text{-CeO}_2$, *Sens. Actuat. B* 169 (2012) 261–266.
- [2] L.L. Sui, Y.M. Xu, X.F. Zhang, X.L. Cheng, S. Gao, H. Zhao, Z. Cai, L.H. Huo, Construction of three-dimensional flower-like $\alpha\text{-MoO}_3$ with hierarchical structure for highly selective triethylamine sensor, *Sens. Actuat. B* 208 (2015) 406–414.
- [3] W.H. Zhang, W.D. Zhang, Fabrication of $\text{SnO}_2\text{-ZnO}$ nanocomposite sensor for selective sensing of trimethylamine and the freshness of fishes, *Sens. Actuat. B* 134 (2008) 403–408.
- [4] Y.J. Xie, J.P. Du, R.H. Zhao, H.Y. Wang, H.L. Yao, Facile synthesis of hexagonal brick-shaped SnO_2 and its gas sensing toward triethylamine, *J. Environ. Chem. Eng* 1 (2013) 1380–1384.
- [5] E. Filippo, D. Manno, A. Buccolieri, A. Serra, Green synthesis of sucralose-capped silver nanoparticles for fast colorimetric triethylamine detection, *Sens. Actuat. B* 178 (2013) 1–9.
- [6] A. Martucci, D. Buso, M.D. Monte, M. Guglielmi, C. Cantalini, C. Sada, Nanostructured sol-gel silica Xphth films doped with NiO and SnO_2 for gas sensing applications, *J. Mater. Chem.* 14 (2004) 2889–2895.
- [7] H.R. Kim, K.I. Choi, K.M. Kim, I.D. Kim, G. Cao, J.H. Lee, Ultra-fast responding and recovering $\text{C}_2\text{H}_5\text{OH}$ sensors using SnO_2 hollow spheres prepared and activated by Ni templates, *Chem. Commun.* 46 (2010) 5061–5063.
- [8] X. Chen, Z. Guo, W.H. Xu, H.B. Yao, M.Q. Li, J.H. Liu, X.J. Huang, S.H. Yu, Templating synthesis of SnO_2 nanotubes loaded with Ag_2O nanoparticles and their enhanced gas sensing properties, *Adv. Funct. Mater.* 21 (2011) 2049–2056.
- [9] K.I. Choi, H.R. Kim, J.H. Lee, Enhanced CO sensing characteristics of hierarchical and hollow In_2O_3 microspheres, *Sens. Actuat. B* 138 (2009) 497–503.
- [10] X. Liu, J. Zhang, X. Guo, S. Wu, S. Wang, Enhanced sensor response of Ni-doped SnO_2 hollow spheres, *Sens. Actuat. B* 152 (2011) 162–167.
- [11] Q. Kuang, C. Lao, Z.L. Wang, Z. Xie, L.S. Zheng, High-sensitivity humidity sensor based on a single SnO_2 nanowire, *J. Am. Chem. Soc.* 129 (2007) 6070–6071.
- [12] L. Vayssières, Growth of arrayed nanorods and nanowires of ZnO from aqueous solutions, *Adv. Mater.* 15 (2003) 464–466.
- [13] I. Paulowicz, V. Hrkac, S. Kaps, V. Cretu, O. Lupan, T. Braniste, V. Duppel, I. Tiginyanu, L. Kienle, R. Adelung, Y.K. Mishra, Three-Dimensional SnO_2 nanowire networks for multifunctional applications: from high-temperature stretchable ceramics to ultraresponsive sensors, *Adv. Electron. Mater.* 1 (2015), 1500081.
- [14] Z.F. Dai, G.T. Duan, Z.X. Cheng, L. Xu, T. Li, G.Q. Liu, H.W. Zhang, Y. Lia, W.P. Cai, Janus gas: reversible redox transition of Sarin enables its selective detection by an ethanol modified nanoporous SnO_2 chemiresistor, *Chem. Commun.* 51 (2015) 8193–8196.
- [15] Y. Kaneti, V.Q.D. Zakaria, Z. Zhang, C. Chen, J. Yue, M. Liu, X. Jiang, A. Yu, Solvothermal synthesis of ZnO -decorated $\alpha\text{-Fe}_2\text{O}_3$ nanorods with highly

- enhanced gas-sensing performance toward n-butanol, *J. Mater. Chem. A* 2 (2014) 13283–13292.
- [16] S. Yang, Y.L. Liu, W. Chen, W. Jin, J. Zhou, H. Zhang, G.S. Zakhrova, High sensitivity and good selectivity of ultralong MoO₃ nanobelts for trimethylamine gas, *Sens. Actuat. B* 226 (2016) 478–485.
- [17] N. Yamazoe, Toward innovations of gas sensor technology, *Sens. Actuat. B* 108 (2005) 2–14.
- [18] H.Y. Xu, D.X. Ju, W.R. Li, H.B. Gong, J. Zhang, J.Q. Wang, B.Q. Cao, Low working temperature, fast-response-speed NO₂ sensor with nanoporous-SnO₂/poly-aniline double-layered film, *Sens. Actuat. B* 224 (2016) 654–660.
- [19] H.J. Kim, J.W. Yoon, K.I. Choi, H.W. Jang, A. Umar, J.H. Lee, Ultra-selective and sensitive detection of xylene and toluene for monitoring indoor air pollution using Cr-doped NiO hierarchical nanostructures, *Nanoscale* 5 (2013) 7066–7073.
- [20] J. Cao, Y.M. Xu, L.L. Sui, X.F. Zhang, S. Gao, X.L. Cheng, H. Zhao, L.H. Huo, Highly selective low-temperature triethylamine sensor based on Ag/Cr₂O₃, mesoporous microspheres, *Sens. Actuat. B* 220 (2015) 910–918.
- [21] I.S. Hwang, J.K. Choi, S. Kim, K.Y. Dong, J.H. Kim, B.K. Ju, J.K. Lee, Enhanced H₂S sensing characteristics of SnO₂ nanowires functionalized with CuO, *Sens. Actuat. B* 142 (2009) 105–110.
- [22] Z.Q. Hua, M. Yuasa, T. Kida, N. Yamazoe, K. Shimane, High sensitive gas sensor based on Pd-loaded WO₃ nanolamellae, *Thin Solid Films* 548 (2013) 677–682.
- [23] S.L. Bai, C. Chen, D.F. Zhang, R.X. Luo, D.Q. Li, A.F. Chen, C.C. Liu, Intrinsic characteristic and mechanism in enhancing H₂S sensing of Cd-doped α -MoO₃ nanobelts, *Sens. Actuat. B* 204 (2014) 754–762.
- [24] Y.F. Kang, L.W. Wang, Y.S. Wang, H.X. Zhang, Y. Wang, D.T. Hong, Y.Q. Qv, S.R. Wang, Construction and enhanced gas sensing performances of CuO-modified α -Fe₂O₃ hybrid hollow spheres, *Sens. Actuat. B* 177 (2013) 570–576.
- [25] H.Y. Xu, D.X. Ju, W.R. Li, J. Zhang, J.Q. Wang, B.Q. Cao, Superior triethylamine-sensing properties based on TiO₂/SnO₂ n-n heterojunction nanosheets directly grown on ceramic tubes, *Sens. Actuat. B* 228 (2016) 634–642.
- [26] X. Li, X. Zhou, H. Guo, C. Wang, J. Liu, P. Sun, F. Liu, G. Lu, Design of Au@ZnO yolk-shell nanospheres with enhanced gas sensing properties, *ACS Appl. Mater. Interfaces* 6 (2014) 18661–18667.
- [27] Y. Wang, Z.T. Zhao, Y.J. Sun, P.W. Lia, J.L. Jia, Y. Chen, W.D. Zhang, J. Hua, Fabrication and gas sensing properties of Au-loaded SnO₂ composite nanoparticles for highly sensitive hydrogen detection, *Sens. Actuat. B* 240 (2017) 664–673.
- [28] D.X. Ju, H.Y. Xu, J. Zhang, J. Guo, B.Q. Cao, Direct hydrothermal growth of ZnO nanosheets on electrode for ethanol sensing, *Sens. Actuat. B* 201 (2014) 444–451.
- [29] H.Y. Xu, X.Q. Chen, J. Zhang, J.Q. Wang, B.Q. Cao, D.L. Cui, NO₂ gas sensing with SnO₂-ZnO/PANI composite thick film fabricated from porous nanosolid, *Sens. Actuat. B* 176 (2013) 166–173.
- [30] Z.F. Dai, L. Xu, G.T. Duan, T. Li, H.W. Zhang, Y. Li, Y. Wang, Y.L. Wang, W.P. Cai, Fast-response, sensitivitive and low-powered chemosensors by fusing nanostructured porous thin film and IDEs-microheater chip, *Sci. Rep.* 3 (2013) 1669.
- [31] Z.F. Dai, H. Dai, Y. Zhou, D.L. Liu, G.T. Duan, W.P. Cai, Y. Li, Monodispersed Nb₂O₅ microspheres: facile synthesis, air/water interfacial self-assembly, Nb₂O₅-based composite films, and their selective NO₂ sensing, *Adv. Mater. Interfaces* 2 (2015), 1500167.
- [32] M. Kwoka, L. Ottaviano, M. Passacantando, S. Santucci, G. Czempik, J. Szuber, XPS study of the surface chemistry of L-CVD SnO₂ thin films after oxidation, *Thin Solid Films* 490 (2005) 36–42.
- [33] Y. Masuda, T. Ohji, K. Kato, Tin oxide nanosheet assembly for hydrophobic/hydrophilic coating and cancer sensing, *ACS Appl. Mater. Interfaces* 4 (2012) 1666–1674.
- [34] X.D. Ma, M.Y. Zhao, Q. Pang, M.H. Zheng, H.W. Sun, J. Crittenden, Y.Y. Zhu, Y.S. Chen, Development of novel CaCO₃/Fe₂O₃, nanorods for low temperature 1, 2-dichlorobenzene oxidation, *Appl. Catal. A-Gen* 522 (2016) 70–79.
- [35] S. Yan, G.T. Zan, Q.S. Wu, An ultrahigh-sensitivity and selective sensing material for ethanol: α - γ -Fe₂O₃ mixed-phase mesoporous nanofibers, *Nano. Res.* 11 (2015) 3673–3686.
- [36] Z.F. Dai, C.S. Lee, Y.H. Tian, I.D. Kim, J.H. Lee, Highly reversible switching from P- to N-type NO₂ sensing in a monolayer Fe₂O₃ inverse opal film and the associated P–N transition phase diagram, *J. Mater. Chem. A* 3 (2015) 3372–3381.
- [37] D.X. Ju, H.Y. Xu, Q. Xu, H.B. Gong, Z.W. Qiu, J. Guo, J. Zhang, B.Q. Cao, High triethylamine-sensing properties of NiO/SnO₂ hollow sphere N-N heterojunction sensors, *Sens. Actuat. B* 215 (2015) 39–44.
- [38] S. Park, S. An, Y. Mun, C. Lee, UV-enhanced NO₂ gas sensing properties of SnO₂-core/ZnO-shell nanowires at room temperature, *ACS Appl. Mater. Interfaces* 5 (2013) 4285–4292.
- [39] X. Li, X. Zhou, H. Guo, C. Wang, J. Liu, P. Sun, F. Liu, G. Lu, Design of Au@ZnO yolk-shell nanospheres with enhanced gas sensing properties, *ACS Appl. Mater. Interfaces* 6 (2014) 18661–18667.
- [40] B. Mondal, B. Basumatari, J. Das, C. Roychaudhury, H. Saha, N. Mukherjee, ZnO-SnO₂ based composite type gas sensor for selective hydrogen sensing, *Sens. Actuat. B* 194 (2014) 389–396.
- [41] J.Q. Hu, Y. Bando, Q.L. Liu, D. Golberg, Laser-ablation growth and optical properties of wide and long single-crystal SnO₂ ribbons, *Adv. Funct. Mater.* 13 (2003) 493–496.
- [42] D.X. Ju, H.Y. Xu, Z.W. Qiu, Z.C. Zhang, Q. Xu, J. Zhang, J.Q. Wang, B.Q. Cao, Near room temperature, fast-response, and highly sensitive triethylamine sensor assembled with Au-loaded ZnO/SnO₂ core-shell nanorods on flat alumina substrates, *ACS Appl. Mater. Interfaces* 7 (2015) 19163–19171.
- [43] M. Uda, A. Nakamura, T. Yamamoto, Y. Fujimoto, Work function of polycrystalline Ag, Au and Al, *J. Elec. Spectr. Rela. Phen* 88–91 (1998) 643–648.
- [44] A. Ponzoni, E. Comini, G. Sberveglieri, J. Zhou, S.Z. Deng, N.S. Xu, Y. Ding, Z.L. Wang, Ultrasensitive and highly selective gas sensors using three-dimensional tungsten oxide nanowire networks, *Appl. Phys. Lett.* 88 (2006) 203101.
- [45] M.W. Ahn, K.S. Park, J.H. Heo, J.G. Park, D.W. Kim, K.J. Choi, J.H. Lee, S.H. Hong, Gas sensing properties of defect-controlled ZnO-nanowire gas sensor, *Appl. Phys. Lett.* 26 (2008) 263103–263103.
- [46] Z.J. Lia, Y.W. Huang, S.C. Zhang, W.M. Chen, Z. Kuang, D.Y. Ao, W. Liu, Y.Q. Fu, A fast response & recovery H₂S gas sensor based on α -Fe₂O₃ nanoparticles with ppb level detection limit, *J. Hazard Mater.* 300 (2015) 167–174.
- [47] L.F. Zhu, M.Y. Wang, T.K. Lam, C.Y. Zhang, H.D. Du, B.H. Li, Y.W. Yao, Fast microwave-assisted synthesis of gas-sensing SnO₂ quantum dots with high sensitivity, *Sens. Actuat. B* 236 (2016) 646–653.
- [48] S.H. Yan, S.Y. Ma, W.Q. Li, X.L. Xu, L. Cheng, H.S. Song, X.Y. Liang, Synthesis of SnO₂-ZnO heterostructured nanofibers for enhanced ethanol gas-sensing performance, *Sens. Actuat. B* 221 (2015) 88–95.
- [49] L.L. Wang, Z. Lou, T. Fei, T. Zhang, Enhanced acetone sensing performance of hierarchical hollow Au-loaded NiO hybrid structures, *Sens. Actuat. B* 161 (2012) 178–183.
- [50] D. Wang, X.F. Chu, M.L. Gong, Gas-sensing properties of sensors based on single-crystalline SnO₂ nanorods prepared by a simple molten-salt method, *Sens. Actuat. B* 117 (2006) 183–187.